15th Australasian Fluid Mechanics Conference
The University of Sydney, Sydney, Australia
13-17 December 2004

An Internal Solitary Wave Parameterization for Hydrodynamic Lake Models

L. Boegman, G. N. Ivey and J. Imberger

Centre for Water Research, The University of Western Australia, WA, 6009 AUSTRALIA

Abstract

A laboratory based closure scheme is presented to parameterize the evolution and subsequent degeneration of high-frequency internal waves in geophysical numerical models. These waves are typically not resolved by discretized governing equations. Our results are suitable for inclusion into field-scale hydrodynamic and water-quality models applied to lakes or reservoirs. In such systems the high-frequency waves result from the non-hydrostatic degeneration of the wind forced basin-scale internal seiche and are believed to sustain a quasi-steady flux of 20% of the introduced wind energy to the benthic boundary layer.

Introduction

Reservoirs are constructed to impound water for later release, hydroelectric power generation and flood control. Reservoirs and natural lakes are often subject to water-quality problems, for example those situated in agricultural regions may suffer nutrient loads via runoff that are in excess of the assimilative capacity of the waterbody. A primary tool for diagnosing poor water-quality and formulating remediation strategies is the coupled hydrodynamic and water-quality model [4]. The predictive capability of such models is limited by the ability of the hydrodynamic scheme to simulate the temperature, salinity and physical transport processes affecting the biogeochemical cycle. In turn, practical field-scale hydrodynamic models (e.g. CE-QUAL-W2, DYRESM, ELCOM and POM) are hindered by their inability to resolve small-scale dynamics. Fortuitously, the fundamental energy flux from the surface wind field to the basin-scale internal wave field may be adequately simulated [7]. However, modelling the down-scale degeneration of the basin-scale motions into high-frequency internal waves has not been addressed and remains a challenge to all modellers [6]. This degeneration process is not described by the governing hydrostatic equations [8] and the high-frequency waves typically have wavelengths of order 100 m [1], much smaller than the feasible grid spacing of field-scale hydrodynamic models [6].

The down-scale energy flux has significant implications for hydrodynamic modelling. Laboratory experiments suggest that in most lakes the basin-scale internal waves will degenerate into progressive solitary waves through nonlinear steepening [9]. During this process, up to 20% of the availible potential energy (APE) input by the wind may be found in the solitary wave field [2]. As the high-frequency internal waves shoal upon sloping topography, up to 80% of the incident wave energy may be lost to dissipation and mixing [3] with between 5% and 25% [11] of the incident energy (1% to 5% of the APE) being converted through diapycnal mixing to an irreversible increase in the potential energy of the water column. The localized nature of these mixing events in space and time may strongly influence biogeochemistry within the littoral zone [10].

The aim of this paper is to parameterize the unresolved internal wave dynamics in terms of parameters that are easily computed from the resolved flow (e.g. wind speed and direction, boundary slope, quiescent stratification, etc.). This parameterization must accomplish the following.

- Quantify the energy transfer to progressive high-frequency internal waves.
- Determine the traveltime until the high-frequency internal waves shoal upon sloping topography.
- Quantify the energy loss from the incident high-frequency wave packet and the fraction of energy being converted through diapycnal mixing to an irreversible increase in the potential energy of the water column (mixing efficiency).
- Determine the position upon the slope where the waves break.

To do so we use results from the laboratory experiments by [11], [9], [2] and [3].

The Internal Solitary Wave Parameterization

During the summer months a stratified lake will typically possess a layered structure consisting of an epilimnion, metalimnion and hypolimnion. If the vertical density gradient is abrupt through the metalimnion, the lake may be approximated as a simple two-layer system [9] of depth h_1 and density ρ_1 over depth h_2 and density ρ_2, where $H = h_1 + h_2$ is the total depth and L denotes the basin length. Internal waves may be initiated within a stratified lake by an external disturbance such as a surface wind stress τ. This stress advects surface water toward the lee-shore, thus displacing the internal layer interface through a maximum excursion η_o as measured at the ends of the basin. The excursion is dependent upon the strength and duration of the wind event. A steady state tilt of the interface is achieved when a steady wind blows for at least one quarter of the fundamental seiche period (defined below) [13] and η_o may be calculated from the integral of the shear velocity $u_* = \sqrt{\tau/\rho_o}$ as

$$\eta_o \approx \frac{L u_*^2}{g' h_1}, \tag{1}$$

where ρ_o is a reference density and $g' = g(\rho_2 - \rho_1)/\rho_2$ is the reduced gravity at the interface [12]. To first order, the APE introduced by the tilted interface is given as [2]

$$\mathrm{APE} = \frac{16 g L (\rho_2 - \rho_1) \eta_o^2}{\pi^4}. \tag{2}$$

Upon termination of the wind stress, the period of the fundamental basin-scale internal standing wave (or seiche) for the two-layer system is

$$T_i = \frac{2L}{c_o}, \tag{3}$$

where $c_o = \sqrt{(g' h_1 h_2)/(h_1 + h_2)}$ is the linear long-wave speed.

Moderate forcing ($0.3 < \eta_o/h_1 < 1.0$) results in the development of a nonlinear surge and dispersive solitary wave packet (figure 1) [14, 9, 2]. The temporal development of the nonlinear

surge may be quantified by the nonlinearity parameter defined in [2] as

$$I = \frac{\alpha\eta_o}{c_o}, \tag{4}$$

where the nonlinear coefficient $\alpha = \frac{3}{2}c_o(h_1 - h_2)/(h_1 h_2)$. If the interface is at mid-depth, α vanishes, steepening can not occur and there is no production of solitary waves. As the progressive nonlinear surge steepens, its length scale decreases until non-hydrostatic effects become significant and the wave is subject to dispersion. This occurs as $t \to T_s$, leading to the steepening timescale [9]

$$T_s = \frac{L}{\alpha\eta_o}. \tag{5}$$

Steepening is eventually balanced by dispersion and the surge degenerates into a high-frequency internal solitary wave packet. The horizontal length scale λ of a particular wave is [5]

$$\lambda^2 = \frac{12\beta}{a\alpha}, \tag{6}$$

where the dispersive coefficient $\beta = \frac{1}{6}c_o h_1 h_2$. Note the inverse relationship between the wavelength λ and amplitude a for the nonlinear waves and that $a \sim \eta_o$ [8].

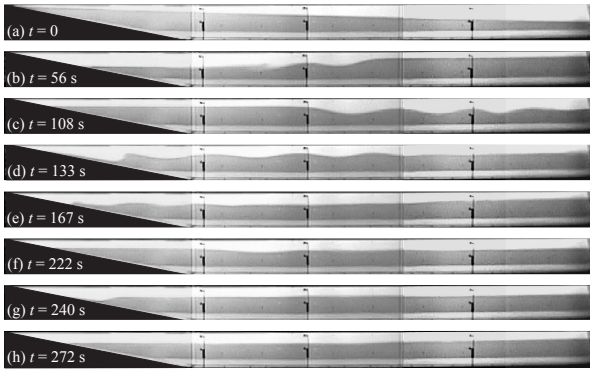

Figure 1: Video frames showing the wave field evolving from the initial condition of upwelling at the slope in (a). The surge and internal solitary wave packet are propagating to the right in (b), (c) and (f) and to the left in (d), (e) and (g). Wave breaking is shown to occur upon the slope. For this experiment $h_1/H = 0.29$ and $\eta_o/h_1 = 0.90$. The apparent dye-free layer near the tank bottom is a spurious artifact of light reflection. Reproduced from [3].

Temporal energy transfer to high-frequency waves

From the laboratory experiments, we have quantified the temporal evolution of the energy in the high-frequency internal solitary waves. This was accomplished by integrating the square of the interfacial displacement associated with the passage of each wave. Interfacial displacement timeseries were recorded using ultrasonic wavegauges as depicted in figure 1. In figure 2a this energy is shown as contours normalized by the APE, where the vertical axis ($\alpha\eta_o/c_o$) indicates the relative magnitudes of the linear and nonlinear components of the internal wave field [3] and the horizontal axis (T_i) reveals how the system evolves in time.

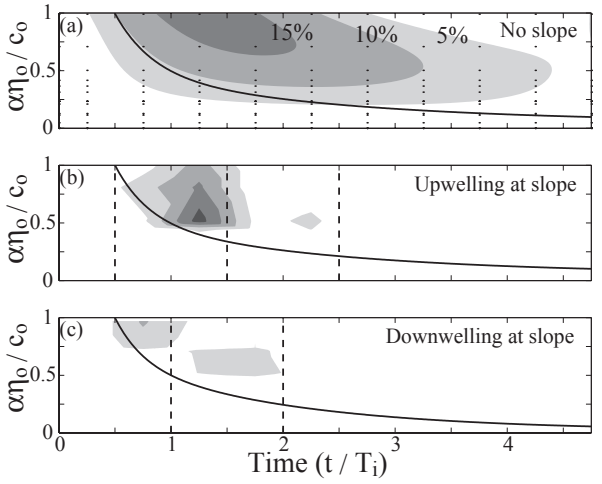

Figure 2: Evolution of the internal wave energy E_{ISW}/APE: (a) Normalized energy for the case of no slope. Contours are least-squares fit to the data points (indicated by $\cdot$) as described in the text. Normalized energy for the initial conditions of (b) upwelling and (c) downwelling along a 0.145 slope. In all panels the contours are presented as a percentage of the APE introduced at $t = 0$ with a contour interval of 5%. The ratio T_s/T_i for a particular $\alpha\eta_o/c_o$ is indicated by —. The times at which the solitary wave packet shoals upon the sloping beach are denoted with – –. Reproduced from [3].

For systems where $\alpha\eta_o/c_o \to 1$, the energy in the solitary waves E_{ISW} is shown to increase to as much as 20% of the APE. For the experiments shown in this figure, the end walls of the domain were vertical, thus favouring wave reflection over breaking and the energy in the solitary wave packet was ultimately lost to viscosity on timescales of order $3T_i$ to $5T_i$. The contours in figure 2a are calculated from the data points through fitting a third-order two-dimensional polynomial to the data in a least-squares sense with a RMS error of 3% of the APE. The equation for the polynomial is

$$\begin{aligned}\frac{E_{ISW}}{\text{APE}} &= 0.0169I^2T_i^3 - 0.0346I^2T_i^2 - 0.1693IT_i^2 \\ &\quad - 0.2624I^2T_i + 0.1714I^2 + 0.0081IT_i^3 \\ &\quad + 0.6896IT_i - 0.2301I - 0.0021T_i^3 \\ &\quad + 0.0259T_i^2 - 0.0821T_i + 0.0292. \end{aligned} \tag{7}$$

Traveltime of the Progressive Internal Waves

The solitary wave packet evolves from the large-scale flow at $t \approx T_s$ (figure 2a and [9]). This packet will first encounter sloping topography after traveltimes of T_s/T_i =0.5, 1.5, 2.5, etc. and T_s/T_i =1, 2, 3, etc. for the initial conditions of upwelling (figure 2b) and downwelling (figure 2c) along the slope, respectively [3]. Clearly, significant energy is lost from the high-frequency internal wave field due to wave breaking at the boundary. The actual time at which a particular solitary wave packet shoals, may be computed as the travletime appropriate to the forcing direction (upwelling or downwelling along the slope) subsequent to $t = T_s$.

Mixing and Dissipation Due to Wave Breaking

The ratio of the beach slope S to the wave slope (a/λ) is commonly used to classify breaking surface waves. This ratio may

be expressed as the off-shore form of the Iribarren number ξ,

$$\xi = \frac{S}{(a/\lambda)^{1/2}}. \quad (8)$$

The Iribarren number has also been shown to be appropriate for internal waves, describing the energy loss along the slope, the mixing efficiency and the breaker type [3]. However, the difficulty in measuring the unresolved parameters λ and a necessitates recasting ξ in terms of the resolved flow variables. To do so a knowledge of the internal wave profile is required.

In figure 3, published observations (as described in [2]) suggest that when the inverse Wedderburn number, which is given for our two-layer system as

$$W^{-1} = \frac{\eta_o}{h_1} \sim \frac{a}{h_1}, \quad (9)$$

is greater than 0.4 the internal solitary waves will have a sech^2 profile and $a/\lambda \sim \alpha\eta_o/c_o$ [2], hence (8) becomes

$$\xi_{\text{sech}} = \frac{S}{(\alpha\eta_o/c_o)^{1/2}}. \quad (10)$$

Conversely for $W^{-1} < 0.4$, the progressive internal waves will have a sinusoidal profile, $a/\lambda \sim f\eta_o/c_o$ and (8) becomes

$$\xi_{\text{sin}} = \frac{S}{(f\eta_o/c_o)^{1/2}}. \quad (11)$$

From figure 3 we take the wave frequency $f \sim 10^{-4}$ Hz.

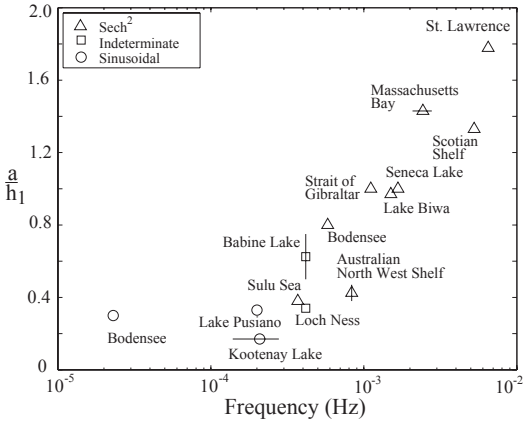

Figure 3: Observations of progressive internal waves as reported in [3]. A relationship between the wave nonlinearity ($a/h_1 \sim \eta_o/h_1$), profile (see legend) and frequency (f) is shown. Reproduced from [3].

The high-frequency internal solitary wave packets have been observed to break upon encountering sloping topography (figure 1). In figure 4, the reflection coefficient $R = E_r/E_i$ (where E_r and E_i are the energy in the reflected and incident wave packets, respectively) and mixing efficiency are expressed as functions of ξ for individual breaking events (data from [11] and [3]). For small ξ, the wave slope is steep relative to S, spilling breakers are observed, $R \to 0$, viscosity dominates and mixing efficiencies are small. Conversely, for waves with very large ξ, $R \to 1$, buoyancy dominates and the collapsing breakers again induce minimal mixing. Intermediate to these extremes inertia dominates and plunging breakers develop with gravitational instabilities that drive mixing efficiencies peaking near 25%. As the incident waves contain as much as 25% of the APE, it implies that 6% of the APE may be converted by diapycnal mixing to an irreversible increase in potential energy in the near boundary regions.

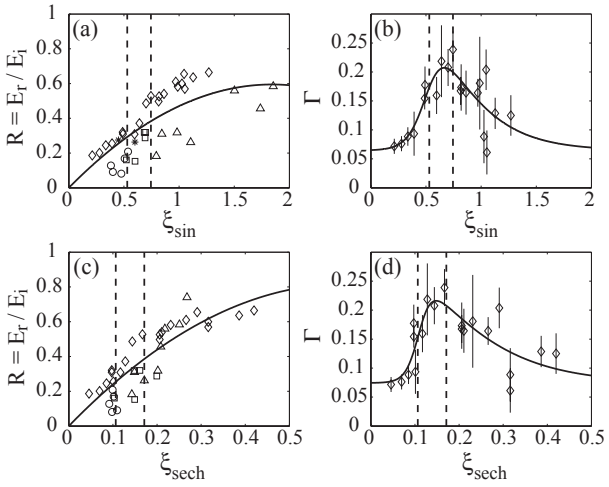

Figure 4: Reflection coefficient (R), mixing efficiency (Γ) and breaker type classified according to the various forms of the Iribarren number: (a) breaker type and R versus ξ_{sin}, (b) breaker type and Γ versus ξ_{sin}, (c) breaker type and R versus ξ_{sech} and (d) breaker type and Γ versus ξ_{sech}. The $--$ lines demarcate the breaker classifications and are inferred in panels b and d from panels a and c, respectively. The lines of best fit are described in the text and the symbols are: ($\circ$) spilling breakers, ($\triangle$) collapsing breakers, ($\square$) plunging breakers, ($\diamond$) from [11] and (*) Lake Pusiano. Reproduced from [3].

Using the least-squares regressions presented in figure 4, both R and Γ may easily be evaluated for a particular ξ. The regressions are

$$R(\xi) = a_1\xi^2 + a_2\xi \quad (12)$$

and

$$\Gamma(\xi) = b_1 + b_2\left(\frac{1}{1+\exp\left[\frac{-(\xi-b_3+b_4/2)}{b_5}\right]}\right) \times \left(1 - \frac{1}{1+\exp\left[\frac{-(\xi-b_3-b_4/2)}{b_6}\right]}\right). \quad (13)$$

In figure 4a and 4b ($W^{-1} < 0.4$ and $\xi \equiv \xi_{\text{sin}}$), a = [-0.1751 0.6454] and b = [0.0646 0.4863 0.4913 -0.0747 0.0820 0.3385]. In figure 4c and 4d ($W^{-1} > 0.4$ and $\xi \equiv \xi_{\text{sech}}$), a = [-2.0852 2.6105] and b = [0.0744 0.3967 0.1019 -0.0186 0.0147 0.1198]. Note that the standard error associated with (12) is approximately $\pm$ 0.1.

Breaker Position

As a wave travels along the slope it steepens, a increases and the streamlines approach vertical. During steepening, the maximum horizontal fluid velocity in the direction of wave propagation will increase more rapidly than the wave velocity and a limiting amplitude may be achieved where the velocities in the wave crest become equal to the phase velocity. This limit is defined as the *breaking limit* and the location on the slope where this limit is observed is the *breaking point*. In [3] the breaking limit is shown to occur along the slope where $a \sim h_1$ (figure 5). Assuming the wave-slope interaction is sufficiently rapid that mixing and reflection do not occur prior to wave breaking, the breaking limit may be found for an initial wave characterized by the off-shore parameters a and λ (ie. $a\lambda$ = constant [3]). Progressing incrementally along the slope in x according to $h_2' = H - h_1 - (H/L_s)x$, where L_s is the slope length and the $'$ denotes a quantity that is variable in x, we discretely evaluate c_o', α' and β' with h_1 = constant. Substitution into (6) gives

$$\lambda' = \frac{12\beta'}{\alpha' a \lambda} \tag{14}$$

which may be rearranged as

$$a' = \frac{12\beta'}{\alpha'\lambda'^2}. \tag{15}$$

Note the transformation of the wavelength-amplitude dependence in (6) to a wavelength-initial condition dependence in (14). Assuming the off-shore wave characteristics may be approximated as $a \sim \eta_o$ and $\lambda \sim c_o/(10^{-4}\text{Hz})$ for $W^{-1} < 0.4$ or $\lambda \sim \sqrt{12\beta/\eta_o\alpha})$ for $W^{-1} > 0.4$, equations (14) and (15) may be used to determine the location x along the slope where the breaking limit $a' \sim h_1$ occurs.

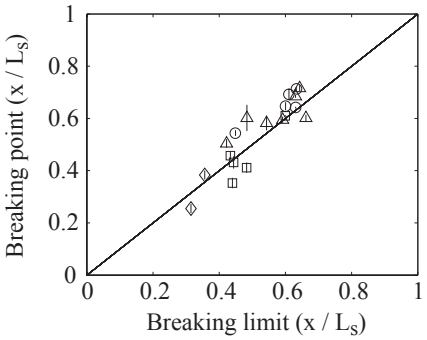

Figure 5: Theoretical breaking limit versus measured breaking point. The breaking limit is determined as the position on the slope where $a' \sim h_1$ from (14) and (15). The symbols are as follows: (○) spilling breakers, (△) collapsing breakers, (□) plunging breakers, (◇) shoaling undular jump. Error bars denote uncertainty in determining the breaking point due to parallax (shows maximum and minimum position). Reproduced from [3].

Conclusions

We have presented a parameterization for the inclusion of high-frequency intenal waves into hydrodynamic lake models. This scheme accounts for the generation, propagation and breaking of the waves at the lake boundary. The parameterization is in terms of the resolved time averaged quantities h_1, h_2, ρ_1, ρ_2, the longitudinal wind direction (ie. upwelling or downwelling along the slope), the integral of τ over $t > T_i/4$ and the basin morphology L and S.

Acknowledgements

We thank David Horn and Hervé Michallet for the raw data used to generate figure 2a and figure 4b and d, respectively. This research has been funded by the Australian Research Council. This paper forms CWR reference ED-1867-LB.

References

[1] Boegman, L., Imberger, J., Ivey, G. N. and Antenucci, J. P., High-frequency internal waves in large stratified lakes, *Limnol. Oceanogr.*, **48**, 2003, 895–919.

[2] Boegman, L., Ivey, G. N. and Imberger, J., The energetics of large-scale internal wave degeneration in lakes, *J. Fluid Mech.*, (Accepted).

[3] Boegman, L., Ivey, G. N. and Imberger, J., Experiments on shoaling internal waves in closed basins, *Limnol. Oceanogr.*, (Accepted).

[4] Chapra, S. C., *Surface water-quality modeling*, McGraw-Hill, 1997.

[5] Djordjevic, V. D. and Redekopp, L. G., The fission and disintegration of internal solitary waves moving over two-dimensional topography, *J. Phys. Oceanogr.*, **8**, 1978, 1016–1024.

[6] Hodges, B. R., Imberger, J., Laval, B. and Appt, J., Modeling the hydrodynamics of stratified lakes, in proceedings *Hydroinformatics Conference*, Iowa Institute of Hydraulic Research, 2000.

[7] Hodges, B. R., Imberger, J., Saggio, A. and Winters, K., Modeling basin-scale internal waves in a stratified lake, *Limnol. Oceanogr.*, **45**, 2000, 1603–1620.

[8] Horn, D. A., Imberger, J. and Ivey, G. N., Internal solitary waves in lakes - a closure problem for hydrostatic models, in proceedings *11th Aha Huliko Hawaiian winter workshop - Internal gravity waves II*, University of Hawaii, 1999.

[9] Horn, D. A., Imberger, J. and Ivey, G. N., The degeneration of large-scale interfacial gravity waves in lakes, *J. Fluid Mech.*, **434**, 2001, 181–207.

[10] MacIntyre, S., Flynn, K. M., Jellison, R. and Romero, J. R., Boundary mixing and nutrient fluxes in Mono Lake, California, *Limnol. Oceanogr.*, **4**, 1999, 512–529.

[11] Michallet, H. and Ivey, G. N., Experiments on mixing due to internal solitary waves breaking on uniform slopes, *J. Geophys. Res.*, **104**, 1999, 13467–13477.

[12] Monismith, S. G., Wind-forced motions in stratified lakes and their effect on mixed layer shear, *Limnol. Oceanogr.*, **30**, 1985, 771–783.

[13] Spigel, R. H. and Imberger, J., The classification of mixed-layer dynamics in lakes of small to medium size, *J. Phys. Oceanogr.*, **10**, 1980, 1104–1121.

[14] Thorpe, S. A., Asymmetry of the internal seiche in Loch Ness, *Nature*, **231**, 1971, 306–308.